ELSEVIER

S0032-3861(96)00571-X

Polymer Vol. 38 No. 4, pp. 785–794, 1997

0032-3861/97/$17.00+0.00

Prediction and manipulation of the phase morphologies of multiphase polymer blends: 1. Ternary systems

H. F. Guo, S. Packirisamy*, N. V. Gvozdic and D. J. Meier†
Michigan Molecular Institute, Midland, MI 48640, USA
(Received 12 October 1995; revised 25 April 1996)

The dispersed phases of a multiphase polymer blend will either form an encapsulation-type phase morphology or the phases will remain separately dispersed, depending on which morphology has the lower free energy. We have developed a model to predict phase morphologies of multiphase polymer blends. Calculations based on the model suggest that interfacial tensions play the major role in establishing the phase structure of a multiphase system, with a less significant role played by the surface areas of the dispersed phases. The model further shows that the phase structure of a multiphase polymer blend can be converted from one type to another by changing the interfacial tensions between one or more pairs of the components using interfacially-active agents such as block or graft copolymers. We have applied the model to different ternary blends of polystyrene, polyethylene, polypropylene and poly(methyl methacrylate), and have compared the predicted morphologies of these blends with experimental results. In each case, the predicted morphologies agree with those found experimentally. In addition, we have successfully converted the phase structures of these blends from one type to another by using interfacially-active block copolymers.

(Keywords: multiphase polymer blends; morphology; phase structure)

INTRODUCTION

Since many advantages can be obtained by the blending of different polymers, polymer blends constitute the fastest growing segment of the plastics industry[1–3]. So far, developments of polymer blends have been mainly focused on two-component systems. However, the simple blending of two immiscible polymers seldom results in favourable properties. Such systems typically have relatively large dispersed phases and weak interfacial adhesion, which results in very poor mechanical properties. A common approach to alleviate this problem involves the addition (or the *in situ* formation) of an interfacially-active agent, or so-called compatibilizer to the blend[4–7]. This compatibilizing component is usually a block or a graft copolymer which will migrate to the interface between the two immiscible polymers. Its presence at the interface promotes a finer dispersion, as well as providing 'bonding' between the two phases. Compatibilization of polymer blends to modify the interfacial properties of blends has been widely investigated and is applied in practice.

Recently, some attention has been drawn to systems having more than two phases[8]. This effort results from the commercial need for new materials, as well as from the possibility that multi-component commingled waste plastics can be recycled into useful products without extensive separation.

In studies of multi-component polymer blends of more than two phases, one of the major interests is to understand and control the phase morphology. Hobbs *et al.* first reported a study on phase morphologies of blends having three co-existing phases[9]. They observed that for some systems one of the minor components formed an encapsulating layer around domains of another minor component (encapsulation-type morphology), whereas in other systems the two minor components formed independent phases (separation-type morphology). Recent studies have shown that the ultimate mechanical properties of multiphase polymer blends are greatly influenced by their phase morphologies[10]. Hence, it is important to understand the factors controlling the phase structures of multi-component systems in order to predict and possibly control them by compatibilization technologies.

Hobbs *et al.*[9] used Harkin's spreading coefficient concept[11] to interpret their observations on the phase morphology of different ternary blends. For a ternary system with A as the continuous phase and B and C as the dispersed phases, the spreading coefficient λ_{BC} of the B-phase on the C-phase is simply

$$\lambda_{BC} = \gamma_{AC} - \gamma_{AB} - \gamma_{BC} \quad (1)$$

where γ_{ij} is the interfacial tension between the i and j phases. If λ_{BC} is positive, the B-phase will encapsulate the C-phase. Similar treatment gives the spreading coefficient of the C-phase on the B-phase

$$\lambda_{BC} = \gamma_{AB} - \gamma_{AC} - \gamma_{BC} \quad (2)$$

Again, a positive value will lead to encapsulation of the B-phase by the C-phase. If both λ_{BC} and λ_{CB} are

*Present address: Vikram Sarabhai Space Center, Indian Space Research Organization, Trivandrum 695022, India
†To whom correspondence should be addressed

negative, the B- and C-phases will remain separate. Most of the observations by Hobbs *et al.* could be interpreted using these criteria.

Although the use of Harkin's spreading coefficient allowed correct predictions of many of the morphologies observed by Hobbs *et al.*, it is really not an appropriate criterion to be used in predicting the phase behaviour of multiphase polymer blends. The equilibrium phase structure of a multiphase system is determined not by interfacial tensions alone, but rather by the interfacial free energy which represents a combination of interfacial tensions and interfacial areas. We have thus modified these phase concepts to include both interfacial tensions and interfacial areas, and have used the resulting expressions to predict the phase structures of different ternary polymer blends of polyethylene (PE), polypropylene (PP), polystyrene (PS) and poly(methyl methacrylate) (PMMA). The morphologies of actual blends covering a broad range of compositions were examined, and in each case the predicted morphologies were observed. In addition, we have successfully converted the phase structures of these blends from one type to another by using interfacially-active block copolymers.

THEORETICAL

As a rule, nature prefers any system which evolves towards its lowest free energy state. Thus, our model is based on the concept that the phase morphology of a multicomponent polymer system will be that which has the lowest free energy.

For a two-component (1 and 2) system with two homogeneous bulk phases (α, β) and an interfacial layer (σ), the Gibbs free energies of the bulk phases and the interfacial layer are given by the following equations[12]

$$G^k = n_1^k \mu_1 + n_2^k \mu_2 \tag{3}$$

$$G^\sigma = n_1^\sigma \mu_1 + n_2^\sigma \mu_2 + A\gamma \tag{4}$$

where G is the Gibbs free energy, n the number of moles, μ is the chemical potential, A the interfacial area, γ the interfacial tension, and $k = \alpha$ and β. Related equations can be written for any multiphase polymer system (having more than two phases)

$$G = \sum_i n_i \mu_i + \sum_{i \neq j} A_i \gamma_{ij} \tag{5}$$

For a N-component system, there will be $N-1$ interfaces coexisting in the system at the lowest free energy.

For a N-component system ($N > 2$), the number of possible interfaces of the system is

$$m = \frac{N!}{2!(N-2)!} \tag{6}$$

However, since only $N-1$ interfaces can coexist, the actual number of different possible arrangements or phase structures is bigger than 1 and is given by the following equation

$$q = N\left\{\frac{m!}{(N-1)![m-(N-1)]!} - \frac{N[m-(N-1)]!}{(N-1)![m-2(N-1)]!}\right\} \tag{7}$$

For a ternary system, there are two co-existing interfaces and nine possible phase structures. *Figure 1* shows the three possible phase structures when A is the matrix phase and B and C are the dispersed phases (comparable figures can be drawn when B or C is the matrix phase). The figure shows: (i) the B and C form separate phases (B + C); (ii) the C phase is encapsulated by the B phase (B/C); and (iii) the B phase is encapsulated by the C phase (C/B). The Gibbs free energy of each structure from equation (5) is

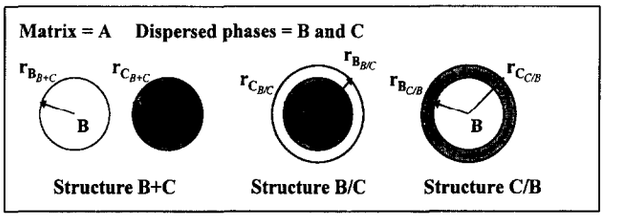

Figure 1 Schematic diagram showing three possible phase structures for a ternary blend at equilibrium: (1) B and C phases remain separate (B + C); (2) the C phase is encapsulated by the B phase (B/C); (3) the B phase is encapsulated by the C phase (C/B)

$$\begin{aligned}
&\text{(i)} \quad G_{B+C} = (n_1\mu_1 + n_2\mu_2 + n_3\mu_3) + (A_{B_{B+C}}\gamma_{AB} + A_{C_{B+C}}\gamma_{AC}) \\
&\text{(ii)} \quad G_{B/C} = (n_1\mu_1 + n_2\mu_2 + n_3\mu_3) + (A_{B_{B/C}}\gamma_{AB} + A_{C_{B/C}}\gamma_{BC}) \\
&\text{(iii)} \quad G_{C/B} = (n_1\mu_1 + n_2\mu_2 + n_3\mu_3) + (A_{B_{C/B}}\gamma_{BC} + A_{C_{C/B}}\gamma_{AC})
\end{aligned} \tag{8}$$

The surface areas of B phase and C phase in three structures are

$$\begin{aligned}
A_{B_{B+C}} &= 3V\Sigma(\phi_{B^i}/r_{B_{B+C^i}}) \\
A_{C_{B+C}} &= 3V\Sigma(\phi_{C^i}/r_{C_{B+C^i}}) \\
A_{B_{B/C}} &= 3V\Sigma\{(\phi_{B^i} + \phi_{C^i})/r_{B_{B/C^i}}\} \\
A_{C_{B/C}} &= 3V\Sigma(\phi_{C^i}/r_{C_{B/C^i}}) \\
A_{B_{C/B}} &= 3V\Sigma(\phi_{B^i}/r_{B_{C/B^i}}) \\
A_{C_{C/B}} &= 3V\Sigma\{(\phi_{B^i} + \phi_{C^i})/r_{C_{C/B^i}}\}
\end{aligned} \tag{9}$$

where V is the total volume, ϕ_B and ϕ_C are volume fractions of B and C phases, and r_{B+C}, $r_{B/C}$ and $r_{C/B}$ are radii of dispersed phases in three structures, as shown in *Figure 1*.

We can predict the phase structure of a ternary polymer blend by comparing the Gibbs free energies of the different structures. Because the $\Sigma n_i\mu_i$ terms in equations (8) are the same, they can be neglected. To further simplify the problem, the surface areas of the minor phases, A_B and A_C, can be calculated based on average phase sizes. The interfacial free energies of the system for different phase structures can be calculated by using the following equations

$$\begin{aligned}
(\Sigma A_i\gamma_{ij})_{B+C} &= (4\pi)^{1/3}\left[n_B^{1/3}x^{2/3}\gamma_{AB} + n_C^{1/3}\gamma_{AC}\right](3V_C)^{2/3} \\
(\Sigma A_i\gamma_{ij})_{B/C} &= (4\pi)^{1/3}\left[n_B^{1/3}(1+x)^{2/3}\gamma_{AB} + n_C^{1/3}\gamma_{BC}\right] \times (3V_C)^{2/3} \\
(\Sigma A_i\gamma_{ij})_{C/B} &= (4\pi)^{1/3}\left[n_B^{1/3}x^{2/3}\gamma_{BC} + n_C^{1/3}(1+x)^{2/3}\gamma_{AC}\right] \times (3V_C)^{2/3}
\end{aligned} \tag{10}$$

where $x = V_B/V_C$, n_B and n_C are numbers of particles of B and C phases in the system. The values of $\Sigma A_i\gamma_{ij}$ will be compared for the three structures and the equilibrium phase structure of the system can then be predicted. In this study we have assumed for simplicity that the number of B and C particles is the same ($n_B = n_C$). We recognized that this may not be true in practice, where the number of particles might differ since a resulting particle size during mixing is the result of the competition between particle break-up and coalescence, and might differ for the two dispersed polymer types. However, results to be presented will show that the predicted morphologies from this simplifying assumption are in remarkable agreement with those observed, so that the assumption seems justified. This is probably the result of the fact that the total surface area of a dispersed phase depends on only the cubic root of the particle number, and hence orders of relative interfacial energies of different phase structures are not very sensitive to the particle numbers of the minor phases.

The prediction procedure is same for systems containing more components. For example, a quaternary system will have a total of 16 possible phase structures with the same matrix component. The Gibbs free energies of different structures can be written based on equation (5), and prediction can then be made by comparing the values $\Sigma A_i\gamma_{ij}$ of the 16 different structures.

EXPERIMENTAL

Materials

The homopolymers used in this study were all commercial products. PS was Styron® 666D from Dow Chemical Company, having the molecular weight of $M_W = 260\,000$ and $M_n = 160\,000$. PMMA having a molecular weight of 90 000 was obtained from Eastman Organic Chemicals (Catalog Number 6036). Isotactic PP was supplied by Amoco Chemical Corporation (Grade Number 1046) with a melt index of 5.8. Two grades of high density polyethylene (HDPE) were used. In the HDPE/PS/PMMA ternary blends, Alathon® H6017 from Occidental Chemical Corporation, with a melt index of 17.5 was used. In the HDPE/PP/PS ternary blends, Tenite® H6001-A from Eastman Chemical Company with a melt index of 8.0 was used.

The poly(styrene-*b*-ethylene) (S-E) and poly(ethylene-*b*-methyl methacrylate) (E-MMA) block copolymers were synthesized in this laboratory by sequential anionic polymerization. The characteristics of these block copolymers are given in *Table 1*.

Table 1 Characteristics of block copolymers

Reference	Structure	Composition	Molecular weight
S-E	PS–PE Diblock	50 wt% PS	73 000
E-MMA	PE–PMMA Diblock	51 wt% PE	79 000

Blend preparations and characterizations

Ternary blends of HDPE/PP/PS and HDPE/PS/PMMA of different compositions were prepared by melt blending in a 60 ml mixer attached to a Haake Rheocord® 90 torque rheometer. Roller blades were used in the mixer. All blending was carried out at 200°C and at 100 rpm for 10 min. After blending, the samples were compression moulded into sheets with a Pasadena hydraulic press at 200°C and 300 psi for 5 min.

For the HDPE/PP/PS ternary blends, the morphologies were examined using transmission electron microscopy (TEM) on sections which were cryomicrotomed from the compression moulded sheets using a LKB 2088 microtome with a diamond knife. The ultra-thin sections were stained with ruthenium tetroxide (RuO_4) vapour for 30 min. The PS phase was heavily stained by the RuO_4, whereas the HDPE and PP phases were only partially stained. Since the degrees of staining were not the same for HDPE and PP, they could be identified by the different staining levels. A Philips TEM (EM301) operated at 80 kV was used to study the microtomed sections.

The morphologies of the HDPE/PS/PMMA ternary blends were studied by scanning electron microscopy (SEM). The compression moulded sheets were fractured in liquid nitrogen, and the resulting fracture surfaces were coated with gold and carbon and examined using an AMRAY 1820 SEM.

RESULTS AND DISCUSSION

HDPE/PP/PS ternary systems

The relative interfacial free energies of ternary blends of HDPE, PP and PS for different phase structures are calculated by using equations (10) and are shown in *Table 2*. In our calculations we assume that $n_B = n_C$ for simplicity. The interfacial tension data used are from Wu[12], and are listed in *Table 3*.

The data shown in *Table 2* indicate that for ternary blends of HDPE/PP/PS having HDPE as the matrix phase, the B/C morphology has the lowest value of $\Sigma A_i\gamma_{ij}$, i.e. the lowest interfacial free energy. Therefore, we would predict that the PS phase will be encapsulated by the PP phase in such blends. In the same manner, we

Table 2 Calculated $\Sigma A_i\gamma_{ij}$ of different ternary HDPE/PP/PS blends

	$\sigma A_i\gamma_{ij}$ (dyne cm)								
Volume ratios of C to B phases (V_c/V_b)	HDPE = A (Matrix), PP = B and PS = C			PP = A (Matrix), HDPE = B, PS = C			PS = A (Matrix), HDPE = B, PP = C		
	B + C	B/C	C/B	B + C	B/C	C/B	B + C	B/C	C/B
2	50.6	50.3	84.1	44.5	56.4	79.9	67.7	67.9	56.7
1	33.9	33.1	70.0	30.0	37.0	67.7	53.2	50.7	44.5
0.5	23.3	22.5	62.1	20.9	25.0	60.9	44.1	40.8	37.7
$\Sigma\gamma_{ij}$ (dyne cm^{-1})	7.0	6.2	11.0	6.2	7.0	11.0	11.0	7.0	6.2

would also predict that in ternary blends of PP/HDPE/PS with PP as the matrix phase, the dispersed HDPE and PS phases will remain separate, whereas in ternary blends of PS/HDPE/PP with PS as the matrix phase, the HDPE phase will be encapsulated by the PP phase.

Experiments were performed to verify these predictions. Blends of HDPE, PS and PP having different compositions were prepared and their morphologies were studied using TEM. *Figure 2* shows a TEM micrograph of a HDPE/PP/PS (70/20/10) blend with HDPE (A) as the matrix phase. We clearly see the spherulitic crystalline texture of the HDPE in the micrograph, and note that particles of PS (C) are encapsulated by PP phases (B). This result is consistent with our prediction based on interfacial energies. It is interesting to note that in *Figure 2* many PS particles appear at the interface between the PP and the HDPE instead of being encapsulated inside the PP phases. It is believed that these PS particles are pushed to the PP/PE interface by the growth fronts of the crystallizing PP, which represents a kinetic factor in establishing phase morphology.

Figure 3 is a TEM micrograph showing the morphology of a PP/HDPE/PS (70/20/10) blend in which PP is the matrix phase. It shows that the HDPE (B) and PS (C) phases remain as separate dispersed phases in the PP matrix (A). The appearances of the dispersed PS and the HDPE particles are different: the HDPE particles have irregular shapes and spherulitic crystalline textures, while the PS particles are more spherical and with smooth surfaces.

Figure 4 shows a TEM micrograph of a PS/PP/HDPE (70/15/15) blend in which PS is the matrix phase. The phase morphology is of the encapsulation type, with the encapsulated inner phase showing a spherulitic crystalline texture similar to that shown by the HDPE phase in *Figure 2*. Thus the inner phase is HDPE (B), with PP (C) being the encapsulating outer layer. Therefore, in each of the three blends, their experimentally observed phase morphologies are in agreement with the theoretically predicted ones.

As mentioned in the Introduction, we have assumed in our predictions that the number of B and C particles is the same, which may not be true because of the complex interplay between shear and interfacial forces in particle break-up. However, calculations based on the actual particle sizes estimated from TEM micrographs of the systems discussed above give results that are essentially the same as those based on the assumption of equal numbers of particles. These results demonstrate that the phase structures of ternary polymer blends can be predicted using our model based on minimizing the interfacial free energy with equal numbers of dispersed B and C particles. We now show that the phase morphologies of these blends can be changed by change of the interfacial tensions between the components. *Figure 5* shows values of $\Sigma A_i \gamma_{ij}$ for the various phase morphologies of ternary blends of HDPE/PP/PS (with HDPE as the matrix component) as a function of $\gamma_{PS/HDPE}$. Crossovers in the interfacial energies of the different phase structures occur as a function of $\gamma_{PS/HDPE}$: at high

Table 3 Interfacial tensions

Interface	Interfacial tension at 140°C (dyne cm^{-1})
PE/PS	5.9
PE/PP	1.1
PP/PS	5.1
PE/PMMA	9.7
PS/PMMA	1.6

Figure 3 TEM micrograph of a PP/HDPE/PS (70/20/10) blend. A = PP, B = HDPE, C = PS

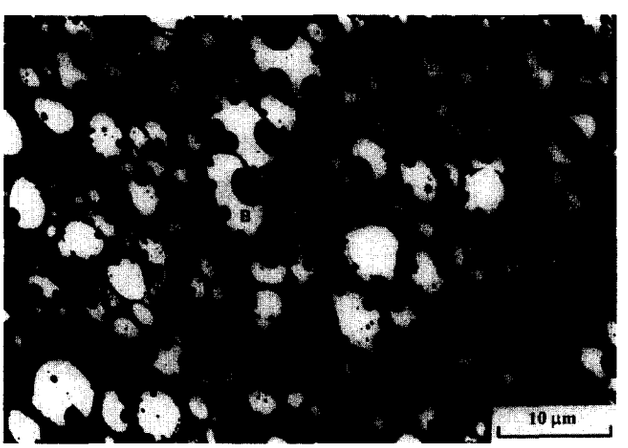

Figure 2 TEM micrograph of a HDPE/PP/PS (70/20/10) blend. A = HDPE, B = PP, C = PS

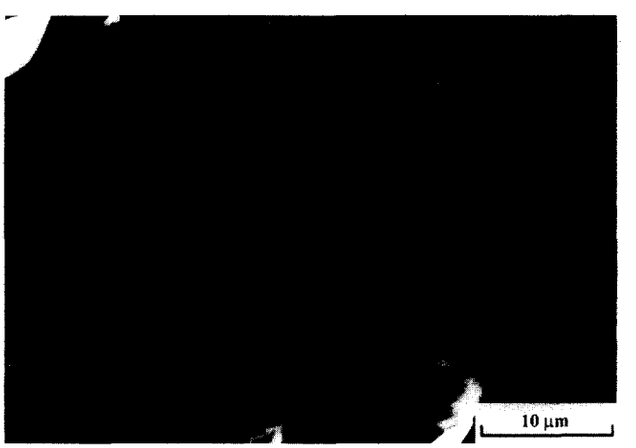

Figure 4 TEM micrograph of a PS/HDPE/PP (70/15/15) blend. A = PS, B = HDPE, C = PP

$\gamma_{PS/HDPE}$ (>5.7 dyne cm^{-1}) the structure PP/PS has the lowest value of $\Sigma A_i\gamma_{ij}$, while at low $\gamma_{PS/HDPE}$ (<5.7 dyne cm^{-1}) the structure PP + PS has the lowest $\Sigma A_i\gamma_{ij}$. The observation suggests that by reducing the interfacial tension $\gamma_{PS/HDPE}$, we can change the phase structure of this ternary system from an encapsulation-type PP/PS to the separation-type PP + PS.

Similarly, we predict that with a reduction in the interfacial tension $\gamma_{PS/HDPE}$, the phase morphology of a PP/HDPE/PS ternary blend with PP as the matrix can be

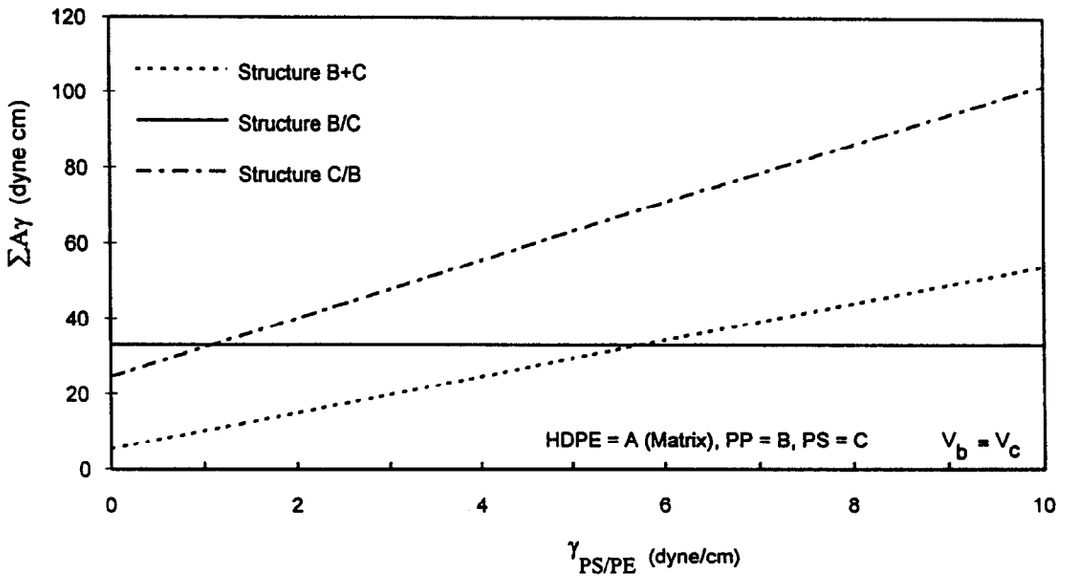

Figure 5 Relative interfacial energies ($\Sigma A_i\gamma_{ij}$) vs interfacial tension $\gamma_{PS/HDPE}$ for ternary HDPE/PP/PS blends where HDPE is the matrix component

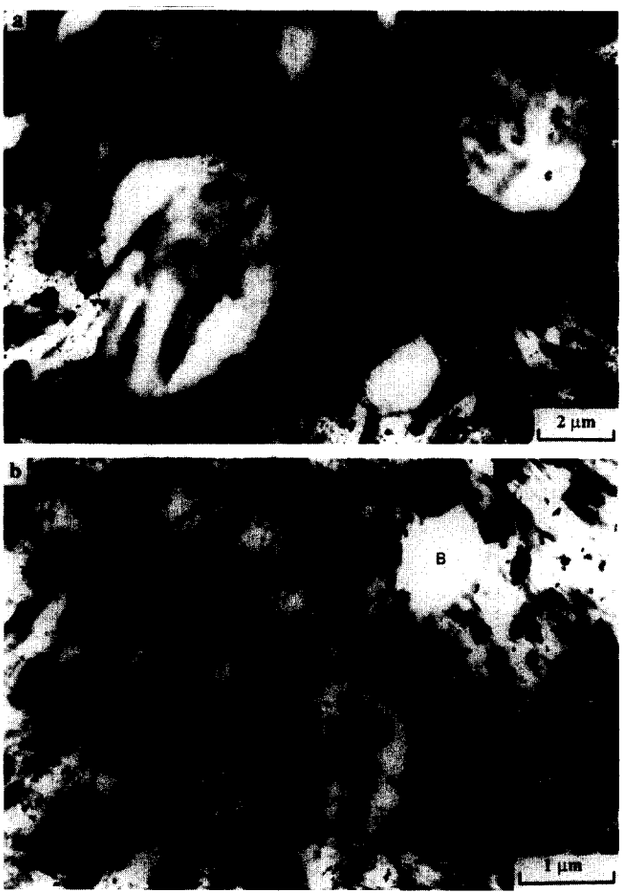

Figure 6 TEM micrographs of a HDPE/PP/PS (70/20/10) blend containing 2% S-E block copolymer: (a) with a magnification of 10 000; (b) with a magnification of 25 000. A = HDPE, B = PP, C = PS

Figure 7 TEM micrographs of HDPE/PP/PS (70/20/10) blends containing: (a) 0.5% S-E block copolymer; (b) 1% S-E block copolymer. A = HDPE, B = PP, C = PS

changed from the separation-type HDPE + PS to an encapsulation-type HDPE/PS. On the other hand, a PS/HDPE/PP ternary blend with PS as the matrix can be changed from the encapsulation morphology PP/HDPE to the opposite encapsulation morphology HDPE/PP.

Experimentally, the reduction in interfacial tension $\gamma_{PS/HDPE}$ was done by adding a small amount of an interfacially-active poly(styrene-*b*-ethylene) (S-E) block copolymer to the blend systems. *Figure 6a* shows a TEM micrograph of a HDPE/PP/PS (70/20/10) ternary blend to which approximately 2 wt% of the S-E block copolymer was added. In contrast to the phase morphology shown in *Figure 2* for this blend without the S-E copolymer, (which shows PS particles encapsulated by PP), *Figure 6a* shows separate PS(C) and PP (B) phases. Thus the phase morphology of this blend has been changed from PP/PS to PP + PS by the addition of the S-E copolymer, i.e. by the reduction in $\gamma_{PS/HDPE}$, and as predicted by our model. It is noted in the micrograph that many tiny particles appear in the HDPE matrix with diameters varying from 400–800 Å, but none in the PP phases. These tiny particles are more clearly shown in TEM micrograph *Figure 6b* having a higher magnification. We believe the small particles are S-E block copolymer micelles, with the larger than expected diameters of such micelles resulting from the solubilization of PS homopolymers into the PS micellar cores.

Figures 7a and *7b* show TEM micrographs of HDPE/PP/PS (70/20/10) ternary blends which contain lesser amounts (0.5 and 1%) of S-E block copolymer to compare with the morphology of this blend system containing 2% S-E and shown in *Figure 6a*. With the addition of only 0.5% S-E, some of the PS (C) particles move to the matrix (A) phase from the PP phase (B), while many of them remain in the interface between the PP and the HDPE phases. On the other hand, when 2% S-E is added, most of the PS particles in the blend are dispersed in the matrix PE phase. Smaller PS particles also result when 1 or 2% S-E block copolymer is added than with the addition of 0.5%. Furthermore, the number of S-E micelles found in the matrix is related to the amount of S-E added, more micelles are found in the samples containing the higher S-E concentrations.

The phase morphology of a PP/HDPE/PS (70/20/10) blend with 1 wt% S-E block copolymer is shown in the TEM micrograph in *Figure 8a*. The separation-type phase morphology (HDPE + PS) shown in *Figure 3* of the system without block copolymer has changed by the addition of the S-E block copolymer to an encapsulation-type (PE/PS) with PS (C) encapsulated by HDPE (B). Block copolymer micelles similar to those in *Figures 6* and *7* are also found in the HDPE phase (B) of this blend, as shown in *Figure 8b*. Although most of the PS particles in this blend are encapsulated in the HDPE phases, some remain in the interface between PE and the PP matrix. The encapsulation of the PS by PE is more complete when 3% S-E block copolymer is added to the system, as shown in *Figure 8c*.

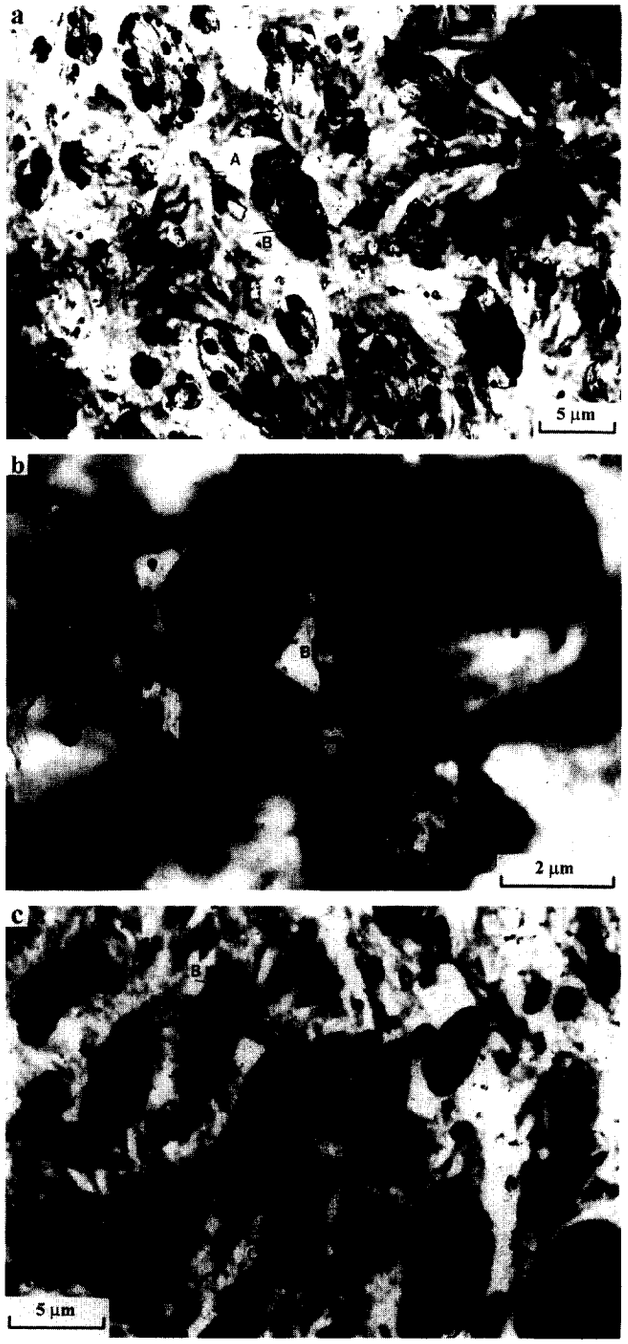

Figure 8 TEM micrographs of PP/HDPE/PS (70/20/10) blends containing: (a) 1% S-E at a magnification of 4000; (b) 1% S-E at a magnification of 15000; and (c) 3% S-E at a magnification of 5000. A = PP, B = HDPE, C = PS

Figure 9 TEM micrographs of a PS/HDPE/PP (70/15/15) blend containing 1% S-E block copolymer. A = PS, B = HDPE, C = PP

Figure 9 shows the phase morphology of a ternary PS/PP/HDPE (70/15/15) blend containing 1% S-E. With the addition of the S-E, the phase structure of this ternary blend changes from the encapsulation of HDPE (B) by PP (C) (*Figure 4*) to the opposite encapsulation of PP by HDPE. The HDPE phase is identified by the similar crystalline type texture seen in *Figure 2*.

Again we have calculated the interfacial free energies

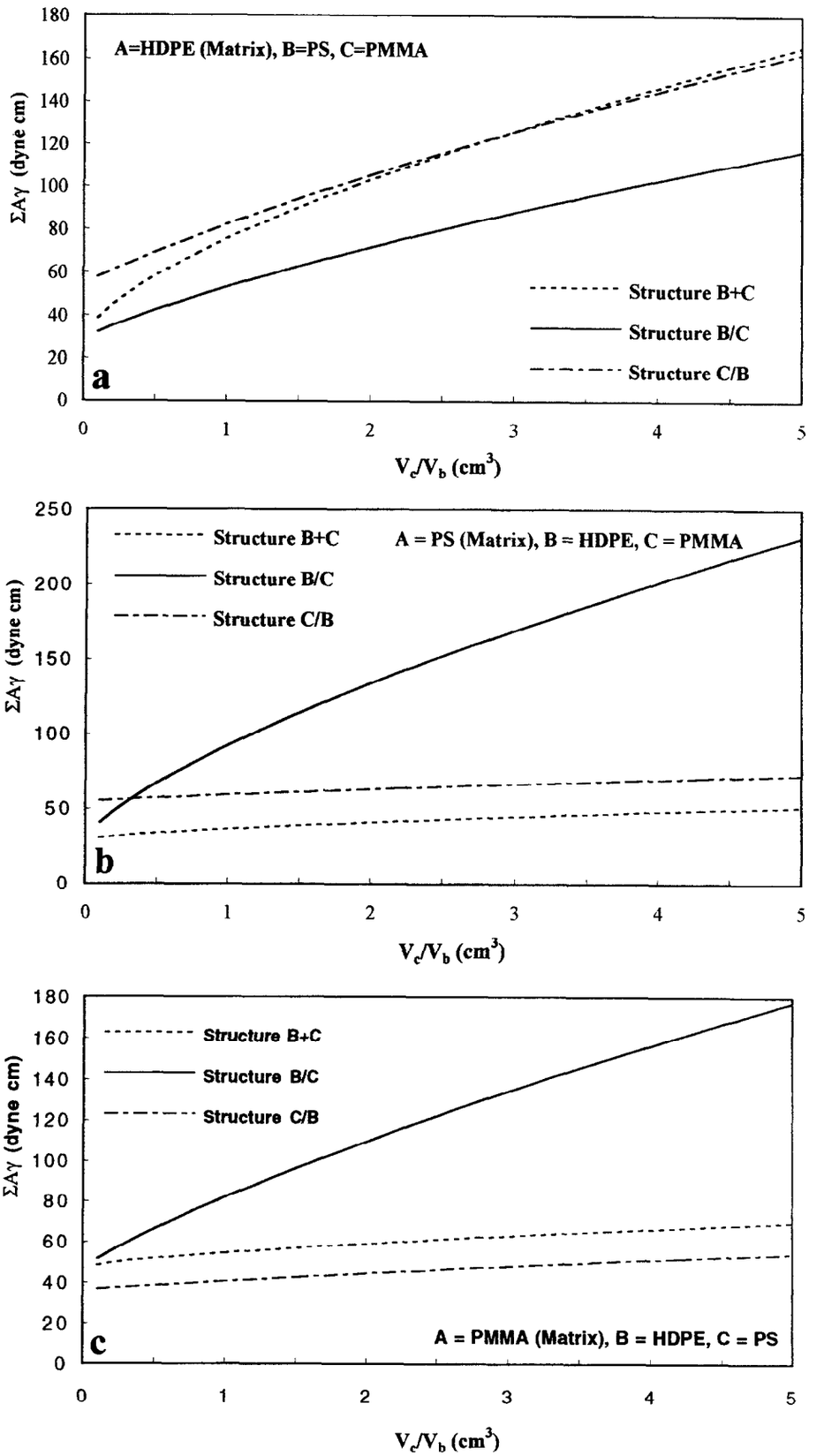

Figure 10 Relative interfacial energies ($\Sigma A_i\gamma_{ij}$) vs volume ratios V_c/V_b for ternary blends of: (a) HDPE/PS/PMMA; (b) PS/HDPE/PMMA; (c) PMMA/HDPE/PS

of these systems using the actual particle sizes estimated from TEM micrographs and have found that the phase structures shown in *Figures 6–9* have the lowest interfacial free energies.

Studies of ternary blends in which LDPE was substituted for HDPE gave similar results to those presented above.

Figure 11 SEM micrograph of the fracture surface of a HDPE/PS/PMMA (70/15/15) blend. A = HDPE, B = PS, C = PMMA

HDPE/PMMA/PS ternary systems

Figure 10 shows $\Sigma A_i\gamma_{ij}$ values for different phase structures and compositions of ternary blends of HDPE, PMMA and PS as a function of the volume ratios of the minor phases. Equations (10) are used in our calculations.

When HDPE is the matrix phase and PS and PMMA are the minor components, the blend will have a phase structure with PMMA encapsulated by PS (PS/PMMA). When PS is the matrix phase and HDPE and PMMA are the minor components, separate dispersions of HDPE and PMMA has the lowest interfacial free energy. Finally, when PMMA is the matrix phase and HDPE and PS are the minor components, the blend is predicted to have the phase structure of HDPE encapsulated by PS.

Experiments verified these predictions. *Figure 11* shows a SEM micrograph of a ternary HDPE/PS/PMMA (70/15/15) blend. Small particles of one minor phase are encapsulated by the other minor phase. Since PMMA is very sensitive to the electron beam of the SEM, we could identify that PMMA was the encapsulated phase (C).

SEM micrographs of a ternary PS/PMMA/HDPE

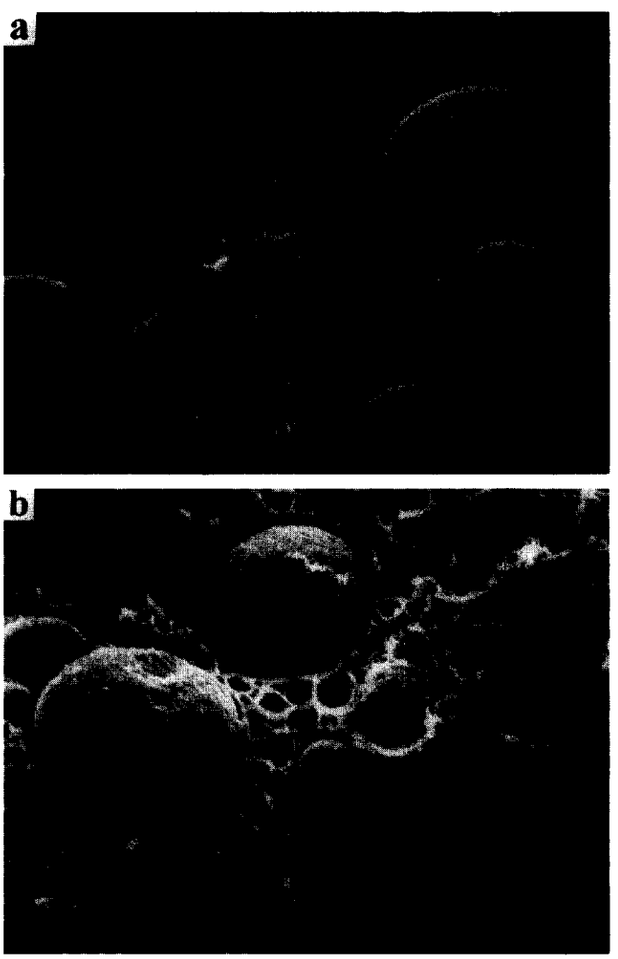

Figure 12 SEM micrographs of a PS/HDPE/PMMA (70/15/15) blend: (a) fracture surface; (b) ethanol/water etched fracture surface. A = PS, B = HDPE, C = PMMA

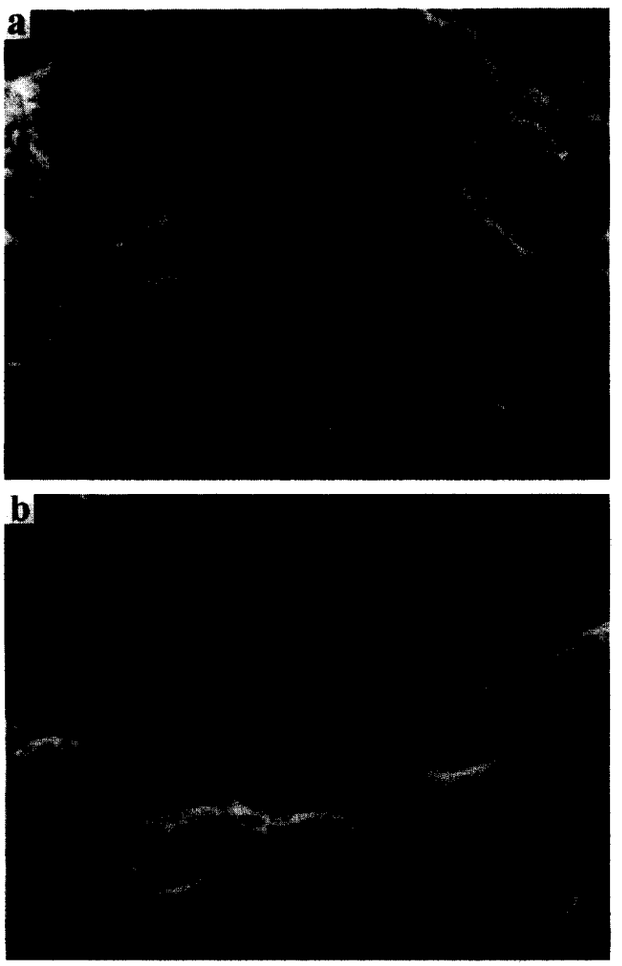

Figure 13 SEM micrographs of a PMMA/HDPE/PS (70/15/15) blend: (a) fracture surface; (b) cyclohexane etched fracture surface. A = PMMA, B = HDPE, C = PS

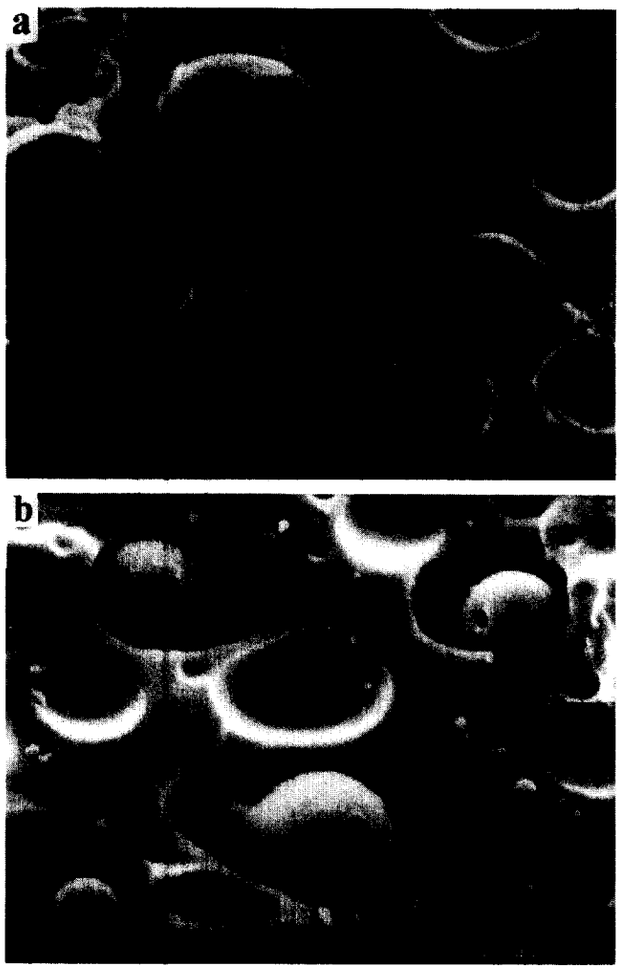

Figure 14 SEM micrographs of a PMMA/HDPE/PS (70/10/20) blend: (a) fracture surface; (b) cyclohexane etched fracture surface. A = PMMA, B = HDPE, C = PS

(70/15/15) blend are shown in *Figure 12*. Two types of particles are dispersed in the matrix, small particles with deformed shapes together with large and small spherical particles. It was shown that the deformation was caused by the electron beam damage, thus identifying the deformed particles as PMMA (C) and the spherical particles as HDPE (B). This identification of the two phases was confirmed by solvent etching of the sample. A fracture surface of the sample was etched with an ethanol/water mixture at 40°C to remove PMMA phase. A SEM micrograph of the resulting surface is shown in *Figure 12b*, and shows that the deformed small particles have disappeared. Therefore, and as predicted, PMMA and HDPE are dispersed separately in this blend.

Figure 13 shows TEM micrographs of a ternary blend of PMMA/PS/HDPE (70/15/15). In *Figure 13a*, particles of one minor phase (B) are surrounded by shells of another minor phase (C) in the matrix of PMMA. To identify these components, the fracture surface of the sample was etched with cyclohexane to remove PS. The SEM micrograph of the etched sample is shown in *Figure 13b*, and shows that all the shells have disappeared. Hence the blend has a phase structure PS/PE with HDPE encapsulated by PS. This morphology is shown even more clearly in *Figures 14a* and *14b*, which show SEM micrographs of a PMMA/PS/HDPE (70/20/10) blend having a higher concentration of PS. The removal of the PS encapsulating phase by etching is clearly apparent.

Figure 15 shows calculated values of $\Sigma A_i\gamma_{ij}$ vs $\gamma_{PMMA/HDPE}$ for different phase structures of ternary blends of PS/HDPE/PMMA, and where PS is the matrix component. Our model predicts that with high $\gamma_{PMMA/HDPE}$ ($>5\,dyne\,cm^{-1}$) the structure HDPE + PMMA has the lowest interfacial free energy, whereas with low $\gamma_{PMMA/HDPE}$ ($<5\,dyne\,cm^{-1}$) the structure PMMA/HDPE has the lowest interfacial free energy. Hence the phase structure of such a blend can be changed by a change of $\gamma_{PMMA/HDPE}$. The interfacially-active

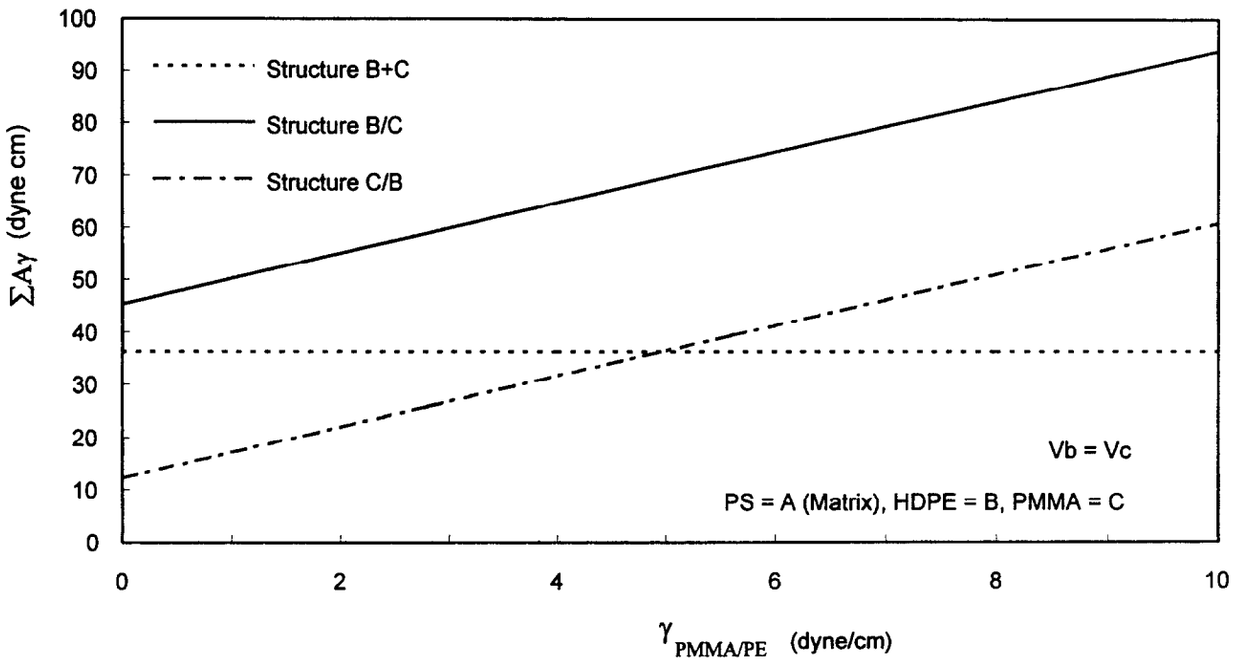

Figure 15 Relative interfacial energies ($\Sigma A_i\gamma_{ij}$) vs interfacial tension $\gamma_{PMMA/HDPE}$ for ternary PS/HDPE/PMMA blends where PS is the matrix component

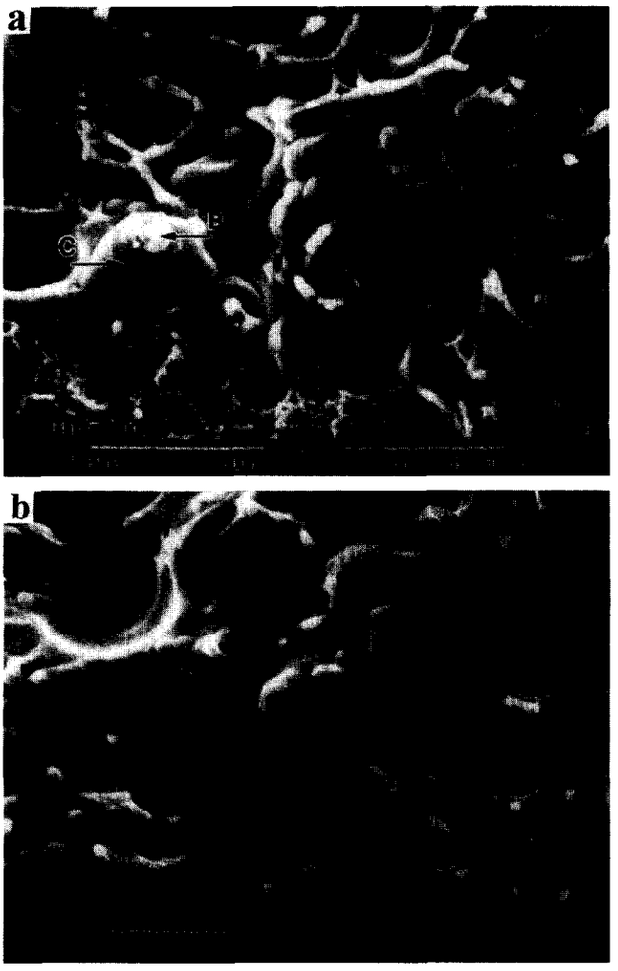

Figure 16 SEM micrographs of a PS/HDPE/PMMA (70/15/15) blend containing 3% E-MMA block copolymer: (a) fracture surface; (b) ethanol/water etched fracture surface. A = PS, B = HDPE, C = PMMA

block copolymer poly(ethylene-*b*-methyl methacrylate) (E-MMA) was used for this purpose. A ternary blend of PS/HDPE/PMMA (70/15/15) containing about 3% E-MMA was prepared. The phase morphology of this blend without E-MMA being present is shown in *Figure 12a*, and shows the HDPE and PMMA phases as separate dispersed phases. In contrast, the morphology of the blend with E-MMA present is shown in *Figure 16a* and shows one of the minor phases partially encapsulated by the other minor phase. An SEM micrograph of a fracture surface after etching with an ethanol/water mixture is shown in *Figure 16b*, and shows that all of the encapsulating layers have disappeared after etching. Thus the encapsulating layer is PMMA and the encapsulated core is HDPE. Thus, as predicted from our model, the phase morphology of this ternary blend can be changed from the separation-type to the encapsulation-type by change of the interfacial tension $\gamma_{PMMA/HDPE}$.

CONCLUSIONS

We have developed a model based on the interfacial free energies to predict the phase morphology of a multiphase polymer blend, and have shown that the predictions are in excellent agreement with experimental results. Calculations based on the model suggest that interfacial tensions play the major role in establishing the phase structure, whereas a less significant (but still important) role is played by the surface areas of the dispersed phases. Our studies furthermore show that the phase structures of multiphase polymer blends can be changed by the addition of suitable interfacially-active agents such as block or graft copolymers.

It is important to point out that our calculations are based on an idealized situation where $n_B = n_C$, whereas the experimental systems may have different particle numbers ($n_B \neq n_C$) due to rheological effects. The agreement between the predicted and experimental results indicates that the orders of relative interfacial free energies of different phase structures are not strongly dependent on the particle numbers or the surface areas of the minor phases. Our results further indicate that the driving force to minimize the free energy is apparently so strong that the phase structure having the lowest free energy level is formed even under the non-equilibrium mixing conditions.

ACKNOWLEDGEMENTS

This work was supported by the National Institute of Standards and Technology under a Department of Commerce Advanced Technology Project grant. We thank Mr Kevin Battjes for his help with SEM and TEM, and Ms Katherine Robertson for her help in photography.

REFERENCES

1 Robeson, L. M. *Polym. Eng. Sci.* 1984, **24**, 587
2 Xanthos, M. *Polym. Eng. Sci.* 1988, **28**, 1392
3 Utracki, L. A. *Polym. Networks Blends* 1991, **1**, 61
4 Paul, D. R. 'Polymer Blends' (Eds D. R. Paul and S. Newman), Vol. 2, Academic Press, New York, 1978, chapter 12
5 Fayt, R., Jerome, R. and Teyssie, P. in 'Multiphase Polymers: Blends and Ionomers' (Eds L. A. Utracki, and R. A. Weiss), ACS, Washington, DC, 1989
6 Fayt, R., Jerome, R. and Teyssie, Ph. *J. Polym. Sci., Polym. Lett.* 1986, **24**, 25
7 Fayt, R., Jerome, R. and Teyssie, P. *Makromol. Chem.* 1986, **187**, 837
8 Debier, D., Devaux, J. and Legras, R. *Polym. Eng. Sci.* 1994, **34**, 613
9 Hobbs, S. Y., Dekkers, M. E. and Watkins, V. H. *Polymer* 1988, **29**, 1598
10 Guo, H. F., Gvozdic, N. V. and Meier, D. J. *PMSE Preprint* 1996, **75**, 444
11 Harkin, W. D. 'The Physical Chemistry of Surface Films', Reinhold, New York, 1952
12 Wu, S. 'Polymer Interface and Adhesion', Marcel Dekker, New York, 1982